***Expression of modified FcγRI enables myeloid cells to elicit robust tumor-specific cytotoxicity***

Leen Farhat-Younis[1], Manho Na[1], Amichai Zarfin[1], Nadine Santana-Magal[1], Alon Richter[1], Aseel Khateeb[1], Amit Gutwillig[1], Diana Rasoulouniriana[1], Annette Gleiberman[1], Lir Beck[2], Tamar Giger[2], Avraham Ashkenazi[3], Adi Barzel[4], Peleg Rider[1], Yaron Carmi[1,5]

[1] Department of Pathology, School of Medicine, Tel Aviv University, Israel

[2] Department of Molecular Cell Biology, Weizmann Institute, Israel

[3] Department of Cell and Developmental Biology, School of Medicine, Tel Aviv University, Israel

[4] Department of Biochemistry Molecular Biology, George S. Wise Faculty of Life Sciences, Tel Aviv University, Israel

[5] Corresponding authors:

Yaron Carmi (yaron.carmi@gmail.com)
Department of Pathology, School of Medicine, Tel Aviv University, Tel Aviv 69978, Israel. Tel: +972-36409504.

Conflict of interest: This work has been supported by Gilboa Therapeutics, of which YC, PR and DR are shareholders. All other authors have declared that no conflict of interest exists.

Grant Support:
This work was funded by the Fritz Thyssen Foundation, the Israel Cancer Research Foundation, and the Israel Science Foundation (ISF) (Grant Number 2262/18).

Running title: Modified FcγR1induce myeloid cell cytotoxicity

**Abstract**

Despite the central role of T cells in tumor immunity, attempts to harness their cytotoxic capacity as a therapy have met limited efficacy, partially as a result of the suppressive microenvironment which limits their migration and activation. In contrast, myeloid cells massively infiltrate tumors and are well adapted to survive in these harsh conditions. While they are equipped with cell-killing abilities, they often adapt an immunosuppressive phenotype upon migration to tumors. Therefore, the questions of how to modify their activation programing against cancer, and what signaling cascades should be activated in myeloid cells to elicit their cytotoxicity has remained unclear.

Here, we found that activation of IgM-induced signaling in myeloid cells results in secretion of lytic granules and massive tumor cell death. These findings open venues for designing novel immunotherapy by equipping monocytes with chimeric receptors that target tumor antigens and consequently, signal through IgM receptor. Nonetheless, we found that myeloid cells do not express the antibody-derived portion used to recognize the tumor antigen due to induction of an ER stress response. To overcome this limitation, we designed chimeric receptors that are based on the high affinity FcγRI for IgG. Incubation of macrophages transfected with these receptors along with tumor-binding IgG induced massive tumor cell killing and secretion of reactive oxygen species and Granzyme B.

Overall, this work highlights the challenges involved in genetically reprograming the signaling in myeloid cells and provides a framework for endowing myeloid cells with antigen-specific cytotoxicity.

## Introduction

Clinical and experimental data have highlighted the important role of the immune cell function and composition in determining tumor progression or eradication (1, 2). While high prevalence of tumor-infiltrating T cells is associated with improved prognosis and survival (3, 4), infiltration of myeloid cells is often associated with poor prognosis and tumor refractory (5, 6). Based on these findings, vast scientific effort is executed to increase the host's T cell response to cancer cells (7, 8). In most cases however, tumor reactive T cells generated spontaneously by the host bear low to moderate affinity ($10^{-4}$M- $10^{-6}$M) (9, 10), which is below the activation threshold needed for therapeutic effect, and attempts to increase TCR affinity using genetical engineering are often limited by induction of cross reactivity (11, 12).

To overcome these limitations, T cells can be genetically modified to express Chimeric Antigen receptor (CAR) consisting of Single Chain Fragment Variable (scFv) for tumor antigen recognition fused to T cell signaling domains (e.g. CD3ζ, CD28) (13, 14). Engineered cells are reinfused into the patient, providing the host's immune system with T cells capable of specifically recognizing tumor antigens in an MHC-independent fashion. Indeed, this strategy benefits from overcoming the complex, multistep and highly regulated activation process of T cells (15, 16) and has been proven remarkably successful in treating liquid tumors.

However, the harsh microenvironment characterizing solid tumors manifests a major limitation to T cell-based treatments. Hypoxic and acidic conditions at tumor sites, along with immunosuppressive capacity of tumor cells limit T cell infiltration, survival, and cytotoxicity (17-19). In contrast to T cells, myeloid cells migrate efficiently into the tumor mass and are well adapted to survive and function under this harsh environment (4, 5). However, while myeloid cells are potentially able to produce cytotoxic compounds, they acquire an immunosuppressive phenotype once in the vicinity of the tumor cells and promote tumor growth (20, 21). Hence, equipping myeloid cells with means to release cytotoxic compounds following recognition of tumor-antigens may provide a new therapeutic strategy. While recognition of tumors can be facilitated through scFv, which signaling chains should be fused are not clear. Early attempts to generate CAR myeloid cells have fused to CD3 zetta chain, which may function in these cells as Fc gamma chain (22, 23). Yet, what signaling cascades should be induced in myeloid cells to elicit their cytotoxicity has remained unclear.

Here, we found that activation of the IgM receptor signaling in myeloid cells, induce massive killing of tumor cells. However, we found that in contrast to lymphoid cells, which can

ectopically express scFv, myeloid cells identify it as a misfolded protein and rapidly degrade it. Instead, we modified the high affinity FcγRI, which normally bind IgG, to transmit IgM receptor-driven signals, while recognition of tumor antigens is mediated by IgG tumor-binding antibodies. Indeed, incubation of mRNA-engineered myeloid cells with tumor cells resulted in massive tumor cell killing only in the presence of IgG tumor-binding antibodies. Overall, this work suggests a novel mean to endow myeloid cells with antigen-specific killing abilities and harness their capacity to migrate and survive in the harsh conditions at the tumor microenvironment.

## *Material and Method*

### *Mice*

Wild-type (WT) C57BL/6 mice were purchased from Envigo (Jerusalem, Israel). C57BL/6-Tg(TcraTcrb)1100Mjb/J OT-I mice were kindly gifted from Prof. Carmit Levy, Tel Aviv University, and B6.Cg-Tg(TcraTcrb)425Cbn/J OT-II mice were generously gifted from Prof. Jakub Abramson, Weizmann Institute, and were housed and maintained in a specific pathogen-free (SPF)conditions animal facility in Tel-Aviv University according to the American Association for the Accreditation of Laboratory Animal. Male and female of 8-12 weeks-old mice were used in all experiments. Animal experiments were approved by the Tel-Aviv University ethics committee.

### *Cell lines*

Human Embryonic Kidney (HEK)-293FT cells were purchased from ThermoFisher Scientific (Waltham, MA, USA). DC 2.4 were a kind gift from Dr. Kenneth Rock Gross from Umass cHAN Medical School. RAW 264.7 were purchased directly from ATCC. THP-1 and U937 were kind gifts from Prof. Mordechay (Motti) Gerlic from the Department of Clinical Microbiology and Immunology at Tel Aviv University. B16F10 (CRL-6475) cells and 4T1 (CRL-2539) cells were directly purchased from ATCC. Cells were cultured in DMEM supplemented with 10% heat-inactivated FBS, 2 mM L-glutamine, and 100 µg/mL penicillin/streptomycin (all from Biological Industries, Israel). All cells were routinely tested for mycoplasma (EZ-PCR Mycoplasma Test Kit, Biological Industries, Israel).

### *Primary cells:*

For bone-marrow DC (BMDC), C57BL/6 mice were sacrificed using a $CO_2$ chamber. Femurs, hip bones, and tibias were obtained and kept in DMEM supplemented with 10% FBS. Bones were washed twice with Phosphate Buffered Saline (Gibco, NY, USA) and sterilized for 10 seconds in a 70% ethanol solution. The cleaned bones were crushed with a sterile mortar and pestle in full medium and the cell mixture was filtered through a 40μM cell strainer. Cells were then centrifuged and resuspended in complete DMEM supplemented with 50 ng/mL GM-CSF and 10 ng/m IL-4 (PeproTech, Rehovot, Israel) and plated at a concentration of $1x10^6$/mL for 6-7 days.

For peritoneal macrophages, C57BL/6 mice were euthanized, and their peritoneum was extensively washed using HBSS (Gibco). Cells were centrifuged and plated overnight in complete DMEM before being subjected to functional experiments.

***Transient transfection:***

**Liposomes-based transfection:** For transfecting HEK293 cells, jetOPTIMUS reagent (Polyplus Transfection, Strasbourg, France) was used according to manufacturer protocol. For DNA transfection of macrophages, Lipofectamine™ 2000 (Invitrogen, Waltham, MA, USA) and jetPEI-Macrophage (Polyplus Transfection) were used.

**Electroporation:** $3x10^6$ cells were suspended in 0.25 mL Opti-MEM medium, mixed with the relevant plasmids, and placed on ice for 20 min in 4 mm cuvettes. Cell electroporation was performed using Gene Pulser Xcell™ electroporation system (Bio-Rad, Hercules, CA, USA). electroporation protocol: voltage - 250V, capacitance 900 μF, resistance ∞ Ω. Immediately following pulsation, cells were washed with pre-warmed DMEM media, centrifuged, and plated in culture plates.

***Production of Lentiviral particles***

$8 \times 10^6$ HEK-293FT cells were plated on a 10 cm plate pre-coated with 200 μg/mL poly-L-lysine and left to adhere overnight and reach a confluence of ~80%. pLVX plasmids containing either receptor of interest tagged with a fluorescent protein or wasabi/ tdTomato control under an EF1 promoter were mixed with psPAX2 (a gift from Didier Trono, Ecole Polytechnique Fédérale de Lausanne, Lausanne, Switzerland; Addgene plasmid 12260) and pCMV-VSV-G (a gift from Bob Weinberg, Massachusetts Institute of Technology, Cambridge, Massachusetts, USA; Addgene plasmid 8454) at a molar ratio of 3:2:1, and cells were transfected using jetOPTIMUS reagent. After 24 hours, the medium was replaced with complete DMEM supplemented with 0.075% sodium bicarbonate. Virus-containing medium was harvested after 24 hours and 48 hours. Following collection, the supernatant was passed through a 0.45μm membrane filter in order to rid it of cellular debris. In order to produce high viral titer stock, viral-containing media was concentrated via centrifugation in Amicon Ultra-15 centrifugal filter unit (100KDa).

***Lentiviral infection***

HEK-293FT cells were transfected with pLVX plasmids containing H2B-tdTomato or HER2 under EF1a promoter together with packaging vector psPAX2 and envelope plasmid pCMV-VSV-G. Media-containing viruses were collected at 24- and 48-hour time intervals. For transduction of tumor cells, cells were incubated with viruses and 100 μg/mL polybrene (Sigma Aldrich, St. Louis, MO, USA) for 30 minutes followed by 30 minutes of centrifugation before medium was replaced. Following three days, cells that expressed $HER2^+$/tdTomato were sorted by FACSAriaII.

***Mouse IgG and IgM purification***

Mouse antibodies were obtained from pooled 5 mL mouse blood obtained from Inferior Vena Cava. Whole blood was left on ice for 20 minutes to allow blood to clot. Blood was then centrifuged at 600 RCF for 10 minutes and serum was collected and re-centrifuged at 20,000 RCF for an additional 10 minutes. Serum was filtered through 0.1 μM and total the IgG and IgM were purified using protein-G and 2-mercaptopyridine columns, respectively (GE Healthcare, Chicago, IL, USA). The levels of purified IgG and IgM were measured with specific ELISA kits (Bethyl, Montgomery, TX, USA) according to manufacturer's instructions.

***Mass Spectrometry***

**Sample preparation** - DC 2.4 were transfected with either αCD19 scFv-GFP or GFP plasmids using Lipofectamine™ 2000 transfection reagent. 4-6 hours post-transfection, when scFv expression was at its maximal level during the expression window (determined by prior calibration experiments), cells were harvested and sorted based on GFP expression using BD FACSAria™ III Cell Sorter. GFP-positive cells collected were resuspended in cell lysis buffer based on PBS + protease inhibitor cocktail (NEB#5871) and lysis was performed using cell sonication (Sonics Vibra Cell VCX 130 Digital Ultrasonic Processor). Sonication protocol: time: 100sec, pulse on: 10sec, pulse off: 10sec, amplitude 25%.

**Protein complex isolation** - Immunoprecipitation was done using GFP-trap magnetic agarose beads (chromotek, Planegg, Germany) according to manufacturer protocol.

Mass spectrometry – (this part of the experiment was performed through a collaboration with Prof. Tami Gieger's lab, Tel Aviv University)

**Sample preparation** – Samples were washed 6 times with washing buffer containing 150mM NaCl and 50mM Tris-HCL (pH 7.5). In every wash, samples were gently rotated in an automatic rotator for 1 minute. Then samples were collected using two rounds of 50ul elution

buffer. First samples were incubated in an elution buffer containing fresh 2M urea, 50mM Tris-HCL (pH7.5), and 1mM DTT for 2 hours at room temperature and then collected in a new tube. Second, on the left beads, a second elution buffer containing 2M urea, 50mM Tris-HCL (pH7.5), and 5mM Choloroacetmide was added for 10 minutes and collected the liquid to the same tube as collected with the first elution and wait 30 minutes. Then we added 5ug/ml trypsin (Promega, Wisconsin, USA) for overnight incubation. Samples were collected in PCR tubes, vacuum dried, and re-suspend in 5ul buffer containing 2% ACN and 0.1% trifluoroacetic acid (TFA).

**LC-MS** - LC-MS/MS runs were performed on the EASY-nLC1000 UHPLC (Thermo Scientific) coupled to Q-Exactive HF mass spectrometers (Thermo Scientific). Peptides were separated with a 75uM X 50 cm EASY-spray column (Thermo Scientific) using a water-acetonitrile gradient of 120 minutes, with a flow rate of 300 ml/min at 40□C. The resolutions of the MS and MS/MS spectra were 60,000 and 15,000 respectively. MS raw files of all samples were jointly analyzed by MaxQuant 2 version 1.6.2.6. MS/MS spectra were referenced to the Uniprot Mus musculus proteome (http://www.uniprot.org/).

**Statistical analysis** – Analyses were performed using the Perseus software 3 version 1.6.2.3.. For the student's t-test results we use a cut-off of FDR < 0.1, S0 = 0.1.

***RT-PCR***

RAW 264.7 cells were transfected with either αCD19 scFv – GFP, GFP control, or additional control containing α chain of FcγRI receptor (CD64) attached to GFP. Transfections were done using JetOPTIMUS according to manufacturer's protocol. 24 hours post-transfection, cells were collected from growth plate using trypsin (Promega). Cells lysis was performed and RNA was purified using RNA NucelSpin RNA manufacturer isolation protocol (Macherey-Nagel, Dueren, Germany). To evaluate RNA sample quality, gel electrophoresis

was performed to detect ribosomal RNA integrity. RNA concentration and purity were tested using NanoDrop One/One$^{C}$ Microvolume UV-Vis Spectrophotometer (ThermoFisher Scientific). – all RNA samples used were at purity levels 260/280 > 2.0, 260/230 between 2.0-2.2.

cDNA was synthesized using qSript cDNA Synthesis Kit (Quantabio, Beverly, MA, USA

| | | |
|---|---|---|
| GFP | Forward primer | AAGTTCAGCGTGTCCGGCGA |
| | Reverse primer | AAGCACTGCACGCCGTAGGT |
| Neomycin | Forward primer | TGAAGCGGGAAGGGACTGGC |
| | Reverse primer | CGAATGGGCAGGTAGCCGGA |
| Mus musculus β-actin | Forward primer | GTCCACCTTCCAGCAGATGT |
| | Reverse primer | GCTCAGTAACAGTCCGCCT |

Quantitative Real-time PCR was conducted using PerfeCTa SYBR® Green FastMix (Quantabio) using stepOne™ Real-Time PCR system. All experiments were done in triplicates.

***mRNA synthesis***

For in vitro capped RNA synthesis pGEM4Z plasmid (kindly gifted from Prof. Eli Gilboa, University of Miami health system) containing T7 promoter along with insert αCD19 scFv – GFP or GFP for control was used as template. Synthesis was performed using AmpliCap-Max™ T7 High Yield Message Maker Kit (Cellscript, Maddison, WI, USA). The synthesis reaction product was tested for integrity via gel electrophoresis. mRNA was purified using NucelSpin RNA.

***mRNA Transfection***

5.0 x $10^4$ RAW264.7 macrophages were plated on 24-well plate a day before the transfection. Synthesized mRNAs were transfected into RAW264.7 using jetMESSENGER RNA

transfection kit (Polyplus) according to the manufacturer's protocol. Transfected cells were analyzed 16-24 hours post-transfection.

***T-cell proliferation assay:***

RAW 264.7 cells were transfected with OVA constructs using Lipofectamine™ 2000. Splenic T cells were isolated from OTI and OTII mice using Ficoll-paque plus density gradient (BD Biosciences, San Jose, CA, USA) followed by incubation with biotin-conjugated anti-$CD8^+$ and anti-$CD4^+$ magnetic beads and magnetic isolation using streptavidin-magnetic beads (BioLegend, Carlsbad, CA, USA). T cells were then labeled with CFSE, washed extensively three times in complete media, and co-cultured at ratios of 1:5 and 1:10 with transfected RAW264.7 cells. After three days, CSFE dilution in T cells was determined by CytoFLEX5.

***Confocal microscopy:***

For confocal microscopy imaging, cells were cultured on glass-bottom confocal plates (Cellvis, Mountain View, CA, USA). Cells were live-imaged or fixed and permeabilized with 2% PFA for 20 minutes. Fixed cultures were washed twice with PBS. For immunofluorescence, fixed cultures were blocked overnight with 5% BSA (ThermoFisher Scientific) and stained with 1:100 or 1:200 diluted primary antibodies. Cells were then washed with PBS containing 1% BSA and stained with a secondary antibody, diluted 1:100 or 1:200. Stains used included: Hoechst 33342 (ThermoFisher Scientific). Lysotracker Deep Red (Invitrogen). ER staining kit - Cytopainter (Abcam, Cambridge, UK). Antibodies for cellular localization assays used included: Anti-GPR78 BiP antibody (Abcam), 20S proteasome β1 antibody(D-9) (Santa Cruz Biotechnology, Dallas, TX, USA), ubiquitin P4D1 mouse monoclonal antibody (mab#3936, Cell signaling technologies, Danvers, MA, USA), G3BP1 antibody (mab#17798, Cell signaling technologies), LC3B antibody (mab#2775, Cell

signaling technologies), and anti-mouse CD64 (FcγRI) (Biolegend). All specimens were imaged by ZEISS LSM800 (ZEISS) and analysed by ZEN 2.3 (ZEISS) and ImageJ.

***Inhibition assays:***

Transfected DC 2.4, RAW 264.7 cells were treated at various time points with various cellular degradation pathway inhibitors: Bafilomycin A1 (Sigma-Aldrich) for autophagy inhibition, MG 132 (Ornat, Rehovot, Israel) – proteasome inhibitor, DBeQ (Sigma-Aldrich) – an inhibitor of p97 ATPase, a component of the ubiquitin-fusion degradation pathway, and Thapsigargin (Sigma Aldrich) – for inhibition of sarco/endoplasmic reticulum $Ca^{2+}$ ATPase (SERCA).

***Flow cytometry:***

Flow cytometry was performed on CytoFLEX5 (Beckman Coulter) using APC-conjugated anti-mouse CD64 (FcγRI), Annexin V and propidium iodide (PI) (all purchased from Biolegend). Data sets were analyzed using FlowJo software (Tree Star, Inc.).

***Killing assay:***

For measuring tumor cell killing, $10^4$ 4T1 H2B-tdTomato, which are genetically modified to express human EGFR or HER2 on cancer cell membranes, were cultured in 96 well plates for 2 hours to adhere. Transfected myeloid cells were added at E:T ratios of 4:1 and 8:1, with or without 10 μg/mL of Trastuzumab (Roche, Basel, Switzerland), Cetuximab (Merck, Darmstadt, Germany), and Rituximab (Genentech, San Francisco, CA, USA). Cells were imaged by IncuCyte S3 imager (Sartorius, Göttingen, Germany), and the numbers of target cells were calculated by incuCyte software. In some experiments, cells were stained with

Annexin V and propidium iodide (PI) (Biolegend) according to manufacturer's instructions, and specific tumor cell lysis was measured by CytoFLEX5.

***Constructs subunits and design process:***

| Construct subunits design | Construct preparation |
|---|---|
| (ssCD8α) – TA99 scFv – CH1 – hinge – CH2 – CH3 – transmembrane + intracellular portion of CD209/ C5α – mCherry | All subunits were designed and designed and ordered in gBlock format from IDT. Integrated DNA Technologies (IDT) (Coralville, IA, USA). Subunits were added to pcDNA 3.1 (+) using Gibson assembly. and cloned to pmCherry- N1. |
| (ssCD8α) – TA99 scFv — CH3 – transmembrane + intracellular portion of CD209/ C5α - mCherry | construct was created by elimination of CH1-hinge-CH2 subunits through invert PCR followed by kinase, ligase, DpnI (KLD) enzymes. |
| pLVX: TA99 scFv – CH3 – (TM+IC) C5α-mCherry | pLVX-IRES-Hyg vector was restricted using SpeI/NotI. Receptor insert including TA99 scFv - heavy chain - C5α (transmembrane + intracellular) - mCherry was restricted from mCherry vector via restriction enzymes NheI/NotI followed by ligation using 4T DNA ligase. |
| (ssCD8α) – CH1 – hinge – CH2 – CH3 – transmembrane + intracellular portion of CD209/ C5α - mCherry | constant heavy sequence, was isolated and amplified using invert PCR for scFv removal followed by KLD enzymes. |
| (ssCD8α) – TA99 scFv - transmembrane and intracellular portion of either CD209 or C5α - mCherry | Removal of constant heavy subunits was done by invert PCR amplification. Followed by KLD enzymes reaction. |
| (ssCD8α) – TA99 scFv – CD8α hinge – CD8α transmembrane – mCherry | Extracellular portion was isolated via restriction with BamHI/EcoRI and inserted into pmCherryN1 vector followed by ligation with 4T DNA ligase |
| (ssCD8α) –CD8α hinge - a | scFv portion was removed via invert PCR using |

| | |
|---|---|
| transmembrane and intracellular portion of either CD209 or C5α - mCherry | Fw primer that included a tail of CD8α hinge sequence as an extracellular remnant. The PCR product was used in KLD enzymes mix reaction. |
| TA99 scFv - GFP | TA99 scFv sequence was restricted from pemCherry-N1 plasmid using EcoRI/XhoI enzymes and inserted to peGFP-N1 plasmid linearized with same enzymes. |
| GFP - T2A - TA99 scFv - mCherry | T2A sequence was designed and ordered in linear gBlock sequence, flanked by restriction enzymes: BglII/NheI. The sequence was inserted to peGFP-C1. GFP-T2A sequence was isolated via restriction with NheI/XhoI and inserted to plasmid which included an insert of TA99 scFv – mCherry. |
| GFP – TA99 scFv – mCherry | Removal of T2A sequence was performed by invert PCR followed by KLD enzyme mix reaction. |
| (ssCD8α) – αCD19 scFv – CD8α hinge – CD8α transmembrane – mCherry | (ssCD8α) – TA99 scFv – CD8α hinge – CD8α transmembrane – mCherry was used as backbone. TA99 was removed by invert PCR amplification exclusion αCD19 scFv was amplified using plasmid pHR-PGK-antiCD19-synNotch-GalVP64 (plasmid#79125) which was purchased from Addgene (Watertown, MA, USA). Both backbone and insert were flanked with XhoI/EcoRI. |
| αCD19 scFv - GFP | αCD19 scFv from plasmid#79125 (Addgene) was amplified using primers with tails encoding restriction sites for XhoI/EcoRI enzymes. peGFP-N1 backbone was restricted using same enzymes. |
| pGEM4Z: T7 promoter - αCD19 scFv – GFP – polyA tail | αCD19 scFv was cloned into pGEM4Z using restriction enzymes NheI + NotI. PGEM4Z GFP was restricted using: XbaI + NheI. |
| pLVX: αCD19 scFv - GFP | αCD19 – GFP was isolated from peGFP-N1 |

| | |
|---|---|
| | backbone using enzymes NheI/NotI and inserted into pLVX backbone linearized using SpeI/NotI |
| GFP - αCD19 scFv | αCD19 scFv sequence was isolated and amplified using primers which included overhang sequence of restriction sites for enzymes XhoI/EcoRI. peGFPC1 was restricted with same enzymes followed by ligation. |
| TA99 variable heavy chain-GFP | Variable heavy chain was isolated and amplified using invert PCR for variable light chin removal followed by KLD enzyme mix. |
| TA99 variable light chain-GFP | Variable light chain was isolated and amplified using invert PCR for variable light chin removal followed by KLD enzyme mix. |
| αCD19 variable heavy chain-GFP | Variable heavy chain was isolated and amplified using invert PCR for variable light chin removal followed by KLD enzyme mix |
| αCD19 variable light chain-GFP | Variable light chain was isolated and amplified using invert PCR for variable light chin removal followed by KLD enzyme mix |
| αCD19 mutated VL (linear) | G-block of mutated αCD19 variable light chain. Two point mutations included replacement of Cysteine amino acid with glycine in positions 24 and 89, flanked by restriction enzymes XhoI/EcoRI was designed and orders from IDT. PeGFP-N1 plasmid was restricted with same enzymes. |
| αCD19 mutated VH (linear) | gBlock of mutated αCD19 variable heavy chain. Two-point mutations included replacement of Cysteine amino acid with glycine in positions 22 and 95, flanked by restriction enzymes XhoI/EcoRI was designed and orders from IDT. PeGFP-N1 plasmid was restricted with same enzymes. |
| LINKER LOOP | DNA sequence was ordered in linear gBlock from |

| | |
|---|---|
| | IDT. Insert of interest was flanked by XhoI/EcoRI and inserted into peGFP-N1 backbone linearized with both enzymes. Final amino acid sequence included: MVTISCRASQDISKYL-GGGGSGGGGSGGGGS-EQEDIATYFCQQGN |
| TA99 scFv – $OVA_{257-264}$ – G4S linker - $OVA_{323-339}$ | DNA sequence including all subunits was designed and ordered in gBlock via IDT. Sequence was inserted into pcDNA 3.1 (+) using restriction enzymes. |
| (ssCD8α) – CD64 – transmembrane + intracellular portion of C5α/CD209/ μ – GFP | CD64 sequence was purchased in gBlock format from IDT, subunits were added in sequence keeping reading frame in check using homology sequences into peGFP-N1. |
| (ssCD8α) – CD64 – transmembrane + intracellular portion of C5α/CD209/μ – T2A - GFP | T2A sequence was ordered in linearized DNA gBlock from IDT. Sequence was flanked by homology sequence which overlapped plasmid ends created by restriction with enzymes BamHI/XmaI. |
| pLVX: (ssCD8α) – CD64 – transmembrane + intracellular portion of C5α/CD209 – T2A GFP | Receptor sequence including all subunits - GFP was isolated from peGFPN1 plasmid using restriction enzymes NheI/NotI. pLVX backbone was linearized using SpeI/NotI. |
| CD64 (extracellular + transmembrane) – GFP (used for RT PCR expression control) | Transmembrane + intracellular sequences were removed from (ssCD8α) – CD64 – transmembrane + intracellular sequence – GFP using invert PCR. Followed by KLD enzymes |

| | |
|---|---|
| | reaction. |

***Table 1.*** *scFv construct design and preparation process*

### *Kits and materials used for cloning*

NucleoSpin Plasmid easy pure (Macherey-Nagel), NucleoSpin Gel and PCR clean-up (Macherey-Nagel), NucleoBond Xtra Maxi (Macherey-Nagel), Zymoclean Gel DNA recovery kit (Zymo research, Irvine, CA, USA). **Cloning**: DH5α Competent cells (Thermo-scientific) were grown in LB broth with agar (Miller) (Sigma Aldrich) or LB broth (Miller) (Merck) supplemented with Ampicillin, sodium salt or Kanamycin sulfate Bio Basic, Markham, Ontario, Canada). **Enzymes and reagents:** Restriction enzymes, T4 DNA ligase, KLD enzyme mix, and Phusion High Fidelity DNA polymerase were purchased from New England biolabs (Ipswich, MA, USA), Taq DNA polymerase mix (PCRBIO, Wayne, PA, USA), RepliQa HiFi Assembly Mix (Quantabio). **Gel electrophoresis:** SeaKem LE agarose (Lonza, Basel, Switzerland)**,** Ethidium Bromide (Merck)**,** TAE buffer (Sartorius, Göttingen, Germany)

### *Statistical analyses*

All statistical analyses and graphs were performed by GraphPad Prism 9. Each experimental group consisted of at least three mice and repeated at least three independent times. Significance of results was determined using the nonparametric one-way ANOVA with Tukey's and Sidak correction, when multiple groups are analyzed, two-way ANOVA with Tukey's and Sidak correction for multiple comparisons.

## Results

### *IgM-induced signaling elicits cytotoxic response in macrophages and can be integrated to a CAR design*

We have previously demonstrated that MHC-matched allogenic tumors, which spontaneously regressed, are coated with IgG and IgM antibodies soon after tumor initiation and are found in proximity to tumor-infiltrating myeloid cells (24). While we characterized the therapeutic role of tumor-binding IgG and their interactions with dendritic cells (DC)(25), the role of IgM in facilitating DC-mediated immunity has remained unclear. To address that, we initially compared their capacity to induce tumor immunity in a prophylactic tumor immunization assay. To this end, we incubated monocyte-derived dendritic cells (MoDC) with immune complexes (IC) composed of B16F10 tumor cells coated with allogenic IgG or IgM and injected them subcutaneously (s.c) to syngeneic mice (illustrated in Fig. 1A). After two rounds of immunization, five days apart, mice were challenged with B16F10 cells and tumor size was monitored over time. We found that incubation of MoDC with IgG-IC, but not with IgM-IC, induced T cell immunity and prevented tumor growth (Fig. 1B). We noticed however, that incubation *in vitro* of MoDC with tumor cells coated with allogenic IgM but not with IgG, resulted in a massive killing of the tumor cells (Fig. 1C). To assess the underlying killing mechanisms, we measured the levels of nitric oxide (NO) and granzyme B (GrB) in the supernatants of overnight cultures. Consistent with their killing rates, significantly higher levels of both GrB and NO were detected upon incubation with allogenic IgM-IC (Fig. 1D), indicating that both secretion of reactive oxygen species and lysosome deposition are involved in the killing. To further assess what signaling cascade is induced by IgM-IC, we tested the levels of major inflammatory cytokines and phosphorylated enzymes. Activation with IgG-IC induced classical singling through Fcγ receptors, characterized by high levels of TNFα and IL12, and activation of enzymes in the MAP kinase pathway (Fig. 1E-1F). The phenotype of IgM-IC activated MoDC was more complicated and characterized in low levels of TNFα and high IL-12, suggesting that Akt was only partially phosphorylated. Flow cytometric analysis indicated only neglectable levels of Akt phosphorylation, while ERK and p38 phosphorylation was comparable to that induced by IgG-IC along with higher levels of phospho-JNK (Fig. 1E-1F). This somewhat unique signaling cascade most likely indicates a combination of several signaling chains recruited by IgM, including Fcγ and C1q receptors.

To harness this signaling cascades to induce tumor cytotoxicity, we designed Chimeric Antigen Receptors (CAR) in which the antigen recognition region, a single chain fragment variable (scFv) derived from TA99 antibody, targets the melanoma antigen gp75, as previously reported (26). The scFv, consisting of Variable light ($V_L$) and variable heavy ($V_H$)

chains was attached to a spacer region of Constant Heavy subunits 1-3 ($CH_{1-3}$). These subunits were fused to several potential IgM signaling chains in the transmembrane and intracellular regions and fused to a fluorescence tag to aid detection of expression (Fig. 1G). Next, we transfected HEK 293FT cells with the CAR constructs to test their expressions and cellular localization using confocal microscopy and flow cytometry. Indeed, all constructs were expressed on cell membrane within 24 hours (Fig. 1H-1I).

***scFv are not expressed by myeloid cells***

Next, we sought to test the constructs expressions and functionality in myeloid cells. To this end, we transfected two established murine cell lines of dendritic cells (DC2.4) and macrophages (RAW 2.64) with our three constructs and with mCherry as a control plasmid. In both cell lines about 30 percent of the cells expressed mCherry. In sharp contrast, however, we were unable to detect any construct expression in myeloid cells by either confocal microscopy or flow cytometric analysis (Fig. 2A-2C and Supplementary Fig. S1A). To test if this phenomenon would also occur in human cells, we transfected THP1 monocyte cell line in comparison to Jurkat T cell line. Consistent with our results using mouse cells, we could not detect any CAR expression in THP1 cells, while in Jurakt cells their expression was comparable to mCherry transfection rates (Fig. 2D-2E).

Since we could not detect expression of our constructs in myeloid cells, we sought to characterize the subunit leading to inhibition of expression by generating various constructs, in which different segments of CAR are omitted. Since myeloid cells were reported to express TRM21 E3 ligases that bind $C_H1$ and $C_H2$ fragments of internalized IgG (27), we next generated a CAR construct with a minimal spacer region by elimination of Constant Heavy domain 1 and 2 ($C_H1$, $C_H2$) and tested the expression of these constructs in DC2.4 cell line. However, consistent with our previous results, we were unable to detect any protein expression (Supplementary Fig. S1B-S1C). We then removed the rest of the spacers, generating a construct consisting only of the scFv region and an intracellular signaling domain. As with our previous finding, no expression in myeloid cell lines was detected (Fig. 2F-2G). Similarly, removal of the intracellular portion did not alter the expression patterns of TA99-derived scFv, suggesting that the scFv domains may be the element that prevents its expression (Fig 2G-2H). To verify that these expression patterns do not stem from the use of mCherry, we have also fused these constructs to GFP. Nonetheless, in both cases the presence of scFv prevented protein expression in macrophages and DC (Supplementary Fig. S1C).

To test if this phenomenon is restricted to TA99 CAR or reflects a broader phenomenon, we sought to compare TA99 CAR to a well-established anti-CD19-derived

scFv. Towards this end, we generated a plasmid that contains the CD8 signal peptide followed by αCD19-derived scFv and fused to CD8a spacer and transmembrane portion, and an identical one that lack the scFv part (Fig. 2H). Interestingly, while we detected low levels of αCD19-derived ScFv, they were localized in intracellular compartments and not on the cell membrane (supplementary Fig. S1D). Removal of scFv domain enabled expression of the inserted protein in the Golgi and cell membrane of both macrophages and DC cells (Fig. 2H-2I and Supplementary Fig. S1E).

***Both VH and VL domains prevent expression of scFv in myeloid cells***

We next aimed to test which portion of scFv prevents its membranal expression. Initially, we designed two plasmids in which all other signaling subunits were removed, leaving only the TA99- or αCD19-derived scFv fragment. As with our previous findings, here too we were not able to detect intracellular TA99- nor αCD19-derived scFv expression (Fig. 3A-3B). To test the possibility that the location of the fluorescent tag inhibits scFv expression, we transfected DC2.4 with a GFP is fused to the C-terminus of αCD19-derived scFv. Similarly, this protein did not lead to scFv expression (Supplementary Fig. S2A). Next, we generated plasmids consisting of minimal subunits, consisting of only the variable light or variable heavy domains of TA99 and αCD19. While expression levels were somewhat higher in these constructs, compared to the full length of scFv, they were still benign and significantly lower compared to GFP only (Fig. 3C-3E).

As a result, we sought to further investigate whether the primary proteins structure of amino acid sequence or the tertiary immunoglobulin structure of the scFv subunits prevent the expression. To this end we inserted point mutations that switched cysteine amino acids to glycine, creating a linear protein by preventing disulfide bonds. Interestingly, linearization of αCD19 variable light chain (or heavy chain) had only marginal effect of its expression patterns and resulted in reduced and compartmentalized expressions (Fig. 3F-3H). In addition, we generated a plasmid that consisted of the first and last 15 amino acids of variable light chain which includes the cysteine amino acids for di-sulfide bond formation. This fragment was almost inert, and its expression patterns were comparable to that of GFP only (Supplementary Fig. S2B). We also tested whether specific fragments within the variable light chain sequence prevented its expression. Dividing the light chains of αCD19 scFv to three sequences resulted in a high expression in myeloid cells, albeit tending to induce different expression patterns of cellular compartmentalization (Figure 3G-3H). Taken jointly, our results suggest that the linear form of either the variable light or the heavy chain of antibodies

results in a poor and compartmentalized protein expression compared to the full length of ScFv to a lesser extent

***scFv induce ER stress in myeloid cells***

To elucidate the level at which scFv constructs are silenced, we sought to transfect cells of myeloid lineage with mRNA composed of αCD19 scFv fused to a green fluorescent protein tag. Nonetheless, this form of transfection did not lead to expression of scFv in myeloid cells (Fig 4A). Additionally, we measured the mRNA levels of GFP mRNA in mouse myeloid cells following transfection with αCD19 scFv-GFP vectors, in comparison to GFP only or to Fc receptor fused to GFP (which are robustly expressed in these cells). Similar levels of GFP mRNA were detected in all transfected cells (Fig 4B.). Based on these findings we speculate that the negative regulation on scFv expression is not evident at the mRNA level.

To further assess this possibility, we utilized 2A ribosomal skipping peptide in order to test if scFv is regulated at the post translational level. Hence, we generated plasmids containing GFP fluorescence tag followed by T2A skipping peptide, succeeded with TA99 scFv fused to mCherry, all in one reading frame. This design allowed us to test if the GFP and scFv expression are coupled, thus indicating that the regulation is made on the mRNA transcript and prior to protein translation. Alternatively, expression of one fluorescent tag would indicate that the regulation is made at the protein level following translation. While we detected both tags (GFP, mCherry) in HEK293 cells, only GFP was expressed in myeloid cells, but not the mCherry which was fused to scFv (Fig. 4C). Eliminating the T2A skipping peptide from this construct, generating a plasmid containing GFP tag fused to TA99 scFv succeeded by mCherry, resulted in abrogated and reduced expression levels of both fluorescent tags in myeloid cells (Fig. 4D). These results therefore suggest that scFv expression is regulated on the protein level.

Consistent with this notion, we found that scFv is expressed in myeloid cell at earlier time points, starting at four hours post transfection and peaking at about 6 hours (Fig. 4E). In order to determine the mechanism through which scFv is degraded, we next performed proteomics of immunoprecipitated scFv. Hence, macrophages were transfected with GFP only, or GFP fused to αCD19 scFv. After 6 hours, GFP-expressing cells were sorted and lysed, and associated proteins were pulled down using anti-GFP conjugated beads. Eluted proteins were then sent to analyses by mass spectrometry (illustrated in Supplementary Fig.S3A). Analysis of protein interactors with scFv in myeloid cells indicated that scFv fraction was statistically enriched with proteins associated with ER stress that could promote

scFv degradation (Fig. 4F). To further corroborate that possibility, we assessed the co-localization scFv with key proteins in this pathway. Confocal microscopy corroborated that the majority of αCD19 scFv were localized at the endoplasmic reticulum (Fig. 4G) and co-localized with BIP (Fig. 4H) and G3BP1(Supplementary Fig.S3B), which are master regulators of ER stress. Lastly, flow cytometric analysis indicated higher levels of phospho-JNK (Fig. 4I).

***FcγRI provides a scaffold for incorporating IgM-induced signaling in myeloid cells and endows them with tumor cell-specific killing ability***

Taking our findings into consideration, we sought to adopt an alternative approach; instead of equipping monocytes with scFv segment, we fused the α chain of the high affinity Fc IgG receptor (FcγRI) as extracellular region fused to signaling chain (Fig. 5A). These construct's recognition of the target cells was designed to be mediated by tumor-binding antibodies. First, we tested the expression levels of the naive and the chimeric FcγRI constructs in RAW264.7 cells. Flow cytometric analysis 24h post transfection indicated that both constructs were successfully expressed at comparable levels (Fig. 5B-5C). Confocal microscopy further indicated that both constructs expressed on the cell membrane and Golgi. (Fig. 5D). Similar expression patterns were also observed in infected murine bone marrow cells (Fig. 5E).

Consequently, we sought to characterize the effect of tumor-binding antibodies on macrophage cytotoxic activity. To this end, we co-incubated tdTomato-labeled 4T1 tumor cell lines expressing human $HER2^+$ with RAW264.7 cells that constitutively express the chimeric receptors with and without the anti-$HER2^+$ antibody *trastuzumab*. Confocal microscopy indicated that RAW264.7 alone had no cytotoxic activity following a 24h incubation. In contrast, the addition of *trastuzumab* induced a polarized accumulation of GrB in the synapse between macrophages and tumor cells. Significantly higher levels of GrB in the immune synapse were counted in cells expressing C5aR chimeric receptor (Fig. 5F-5G and Supplementary Fig. S4A). To quantify the killing capacity of this construct, we next transfected RAW26.4 macrophages with mRNA which encode these modified receptors and incubated them with fluorescently labeled $HER2^+$ expressing 4T1 tumor cells under IncuCyte. Consistent with GrB polarization, transfect macrophages alone were almost completely inert whereas addition of *trastuzumab* promoted tumor cells killing (Fig. 5H). Importantly, while

killing rates of macrophages expressing C5aR chimeric receptor were higher, they were also induced by free and irrelevant antibody (e.g. rituximab) (Fig. 5H).

To assess the underlying mechanism, we analyzed the transfected RAW264.7 cells under high-resolution microscopy. In steady state, cells transfected with the native FcγRI had a clear separation between the alpha chain (antibody binding chain) and their signaling gamma chain. The addition of free trastuzumab did not alter their membranal architecture. Incubation with plastic-immobilized *trastuzumab* resulted in polarization of the alpha chain toward the plastic and co-localization with the gamma chain. The architecture of C5aR chimeric receptor completely abrogated the membrane organization of the signaling chains, as the two co-localized even under steady state (Fig. 5I and Supplementary Fig. S4B). We then speculated that the fusion of such signaling chain to the alpha chain could mitigate the effects of tonic signaling by attaching IgM receptor signaling chain, instead of the gamma chain, to the transmembrane domain (illustrated in Supplementary Fig. 4C). Indeed, this architecture can be highly expressed in macrophage membrane and did not recruit or abrogated the gamma chain upon addition of antibodies, while maintaining alpha chain clustering to immobilized *trastuzumab* (Supplementary Fig. S4D-S4F). Lastly, this construct promotes polarized expression of GrB at the immunological synapse and induces an antibody-specific tumor cell lysis (Fig. 5J-5K).

## Discussion

The microenvironment of most solid tumors is often enriched with myeloid cells at different stages of maturity and polarization and the general notion suggests that they often adapt a suppressive phenotype which support tumor progression and escape (4, 21, 28). The inherent plasticity of these cells, however, enables them to change their phenotype upon injection of adjuvant or immune-stimulatory agents (29-31). Countless experimental and clinical data have been tested for their capacity to convert tumor-infiltrating myeloid cells phenotype to an anti-tumor, including TLR agonists (32-35), immune complexes (24, 36, 37), immune checkpoints (38, 39) and co-stimulatory antibodies (40). While they showed improved T cell infiltration and overall lower tumor burden, they did not meet the expectations. It is noteworthy that most of these attempts are based on the notion that $CD8^+$ T cells are the main effector arm against cancer and that the purpose of myeloid cell activation is to support T cell mediated killing (30, 31). Nonetheless, myeloid cells are highly equipped with cell killing mechanisms, including ADCC, and secretion of reactive oxygen species (41). Here, we demonstrated that activating the IgM-receptor signaling in myeloid cells using tumor-binding IgG induces oxidative burst, Granzyme release, and massive tumor cell lysis.

While genetic engineering of immune cells to treat cancer has proven to be successful in lymphoid cells (16, 42), cells of the myeloid lineage resist gene modification. Noteworthily, these cells are traditionally thought to be programmed to respond to foreign genetic materials. Early attempts to overcome this inherent barrier were achieved by Biglari et al. using adenoviral vectors. They demonstrated that the fusion of scFv against CEA to FcγR can be expressed in monocytes (43). Although this construct leads to granzyme release in T cells, its function in monocytes remained obscure. Further attempts to equip macrophages with specific tumor antigen recognition were done by Morrissey et al. They fused scFv derived from αCD19 antibody to different signaling chains that facilitate phagocytosis (44). Interestingly, most of these receptors do not appear to be expressed on the cell membrane. Moreover, CAR-merTK, which appears on the cell membrane, was functionally inert and did not induce phagocytosis.

Recently, Klichinsky et al. have also attempted to genetically modify macrophages using an adenoviral vector expressing αCD19 and αHER2 Chimeric Antigen Receptor fused to CD3ζ − CD28 signaling domains. They suggested that this strategy can be applied to kill HER2-expressing tumor cells through phagocytosis. While the authors demonstrated expression by flow cytometry, they did not attempt to identify the membranous localization in

macrophages. It may also be that use of Adeno-associated viruses (AAV) as transduction vector enable to overcome the inflammatory cascade induced in myeloid cells as a result of liposome-based transfection or lentiviral transduction, thus enabling expression. With that being said, the authors concluded that the improved survival induced in mice was due to M1-like phenotype induce in transduced macrophages by the virus, rather than the CAR construct (22).

Why scFv induces ER-stress specifically in myeloid cells remains unclear. Activation of ER stress by misfolded proteins in macrophages plays a dominant role in many human pathologies, yet it also occurs in other cell types. One possible explanation is that these cells lack the machinery needed for successful folding of antibody-like structures. Along these lines, many non-immune cells such as HeLa or HEK293 cells initiate ER-stress response upon transfection of fragments derived from immune-associated receptors such as the alpha chain of the T cell receptor (45).

Overall, this work highlights the challenges involved in genetically reprograming the signaling in myeloid cells and the need for new genetic scaffolds other than scFv. Instead, we suggest FcγRI as a new genetic scaffold for modulating myeloid cells signaling as a therapeutic strategy against solid cancer.

## References


1. Coussens LM, Zitvogel L, and Palucka AK. Neutralizing tumor-promoting chronic inflammation: a magic bullet? *Science.* 2013;339(6117):286-91.
2. Fridman WH, Pages F, Sautes-Fridman C, and Galon J. The immune contexture in human tumours: impact on clinical outcome. *Nat Rev Cancer.* 2012;12(4):298-306.
3. Thorsson V, Gibbs DL, Brown SD, Wolf D, Bortone DS, Ou Yang TH, et al. The Immune Landscape of Cancer. *Immunity.* 2018;48(4):812-30 e14.
4. Bruni D, Angell HK, and Galon J. The immune contexture and Immunoscore in cancer prognosis and therapeutic efficacy. *Nature Reviews Cancer.* 2020;20(11):662-80.
5. Greten FR, and Grivennikov SI. Inflammation and Cancer: Triggers, Mechanisms, and Consequences. *Immunity.* 2019;51(1):27-41.
6. Hanahan D, and Coussens LM. Accessories to the Crime: Functions of Cells Recruited to the Tumor Microenvironment. *Cancer Cell.* 2012;21(3):309-22.
7. Fritz JM, and Lenardo MJ. Development of immune checkpoint therapy for cancer. *The Journal of experimental medicine.* 2019;216(6):1244-54.
8. Waldman AD, Fritz JM, and Lenardo MJ. A guide to cancer immunotherapy: from T cell basic science to clinical practice. *Nat Rev Immunol.* 2020;20(11):651-68.
9. Hoffmann MM, and Slansky JE. T-cell receptor affinity in the age of cancer immunotherapy. *Mol Carcinog.* 2020;59(7):862-70.
10. Reuben A, Zhang J, Chiou SH, Gittelman RM, Li J, Lee WC, et al. Comprehensive T cell repertoire characterization of non-small cell lung cancer. *Nat Commun.* 2020;11(1):603.
11. Johnson LA, Morgan RA, Dudley ME, Cassard L, Yang JC, Hughes MS, et al. Gene therapy with human and mouse T-cell receptors mediates cancer regression and targets normal tissues expressing cognate antigen. *Blood.* 2009;114(3):535-46.
12. Casucci M, Hawkins RE, Dotti G, and Bondanza A. Overcoming the toxicity hurdles of genetically targeted T cells. *Cancer Immunol Immunother.* 2015;64(1):123-30.
13. Newick K, O'Brien S, Moon E, and Albelda SM. CAR T Cell Therapy for Solid Tumors. *Annu Rev Med.* 2017;68:139-52.
14. Rafiq S, Hackett CS, and Brentjens RJ. Engineering strategies to overcome the current roadblocks in CAR T cell therapy. *Nat Rev Clin Oncol.* 2020;17(3):147-67.
15. June CH, Maus MV, Plesa G, Johnson LA, Zhao Y, Levine BL, et al. Engineered T cells for cancer therapy. *Cancer Immunol Immunother.* 2014;63(9):969-75.
16. Gross G, and Eshhar Z. Therapeutic Potential of T Cell Chimeric Antigen Receptors (CARs) in Cancer Treatment: Counteracting Off-Tumor Toxicities for Safe CAR T Cell Therapy. *Annual review of pharmacology and toxicology.* 2016;56:59-83.
17. Joyce JA, and Fearon DT. T cell exclusion, immune privilege, and the tumor microenvironment. *Science.* 2015;348(6230):74-80.
18. Hanley CJ, and Thomas GJ. T-cell tumour exclusion and immunotherapy resistance: a role for CAF targeting. *Br J Cancer.* 2020;123(9):1353-5.
19. Lim AR, Rathmell WK, and Rathmell JC. The tumor microenvironment as a metabolic barrier to effector T cells and immunotherapy. *Elife.* 2020;9.
20. Grivennikov SI, Greten FR, and Karin M. Immunity, inflammation, and cancer. *Cell.* 2010;140(6):883-99.
21. Mantovani A, and Sica A. Macrophages, innate immunity and cancer: balance, tolerance, and diversity. *Current opinion in immunology.* 2010;22(2):231-7.
22. Klichinsky M, Ruella M, Shestova O, Lu XM, Best A, Zeeman M, et al. Human chimeric antigen receptor macrophages for cancer immunotherapy. *Nat Biotechnol.* 2020;38(8):947-53.
23. Sloas C, Gill S, and Klichinsky M. Engineered CAR-Macrophages as Adoptive Immunotherapies for Solid Tumors. *Front Immunol.* 2021;12:783305.
24. Carmi Y, Spitzer MH, Linde IL, Burt BM, Prestwood TR, Perlman N, et al. Allogeneic IgG combined with dendritic cell stimuli induce antitumour T-cell immunity. *Nature.* 2015;521(7550):99-104.

25. Carmi Y, Prestwood TR, Spitzer MH, Linde IL, Chabon J, Reticker-Flynn NE, et al. Akt and SHP-1 are DC-intrinsic checkpoints for tumor immunity. *JCI Insight.* 2016;1(18):e89020.
26. Ma L, Dichwalkar T, Chang JYH, Cossette B, Garafola D, Zhang AQ, et al. Enhanced CAR-T cell activity against solid tumors by vaccine boosting through the chimeric receptor. *Science.* 2019;365(6449):162-8.
27. Mallery DL, McEwan WA, Bidgood SR, Towers GJ, Johnson CM, and James LC. Antibodies mediate intracellular immunity through tripartite motif-containing 21 (TRIM21). *Proc Natl Acad Sci U S A.* 2010;107(46):19985-90.
28. Gajewski TF, Schreiber H, and Fu YX. Innate and adaptive immune cells in the tumor microenvironment. *Nat Immunol.* 2013;14(10):1014-22.
29. Quatromoni JG, and Eruslanov E. Tumor-associated macrophages: function, phenotype, and link to prognosis in human lung cancer. *Am J Transl Res.* 2012;4(4):376-89.
30. Ricketts TD, Prieto-Dominguez N, Gowda PS, and Ubil E. Mechanisms of Macrophage Plasticity in the Tumor Environment: Manipulating Activation State to Improve Outcomes. *Front Immunol.* 2021;12:642285.
31. Bercovici N, Guerin MV, Trautmann A, and Donnadieu E. The Remarkable Plasticity of Macrophages: A Chance to Fight Cancer. *Front Immunol.* 2019;10:1563.
32. Cheng H, Sun L, Shen D, Ren A, Ma F, Tai G, et al. Beta-1,6 glucan converts tumor-associated macrophages into an M1-like phenotype. *Carbohydr Polym.* 2020;247:116715.
33. Dudek AZ, Yunis C, Harrison LI, Kumar S, Hawkinson R, Cooley S, et al. First in human phase I trial of 852A, a novel systemic toll-like receptor 7 agonist, to activate innate immune responses in patients with advanced cancer. *Clin Cancer Res.* 2007;13(23):7119-25.
34. Miura K, Ishioka M, Minami S, Horie Y, Ohshima S, Goto T, et al. Toll-like Receptor 4 on Macrophage Promotes the Development of Steatohepatitis-related Hepatocellular Carcinoma in Mice. *J Biol Chem.* 2016;291(22):11504-17.
35. Rodell CB, Arlauckas SP, Cuccarese MF, Garris CS, Li R, Ahmed MS, et al. TLR7/8-agonist-loaded nanoparticles promote the polarization of tumour-associated macrophages to enhance cancer immunotherapy. *Nat Biomed Eng.* 2018;2(8):578-88.
36. Gao CH, Dong HL, Tai L, and Gao XM. Lactoferrin-Containing Immunocomplexes Drive the Conversion of Human Macrophages from M2- into M1-like Phenotype. *Front Immunol.* 2018;9:37.
37. Ackerman SE, Pearson CI, Gregorio JD, Gonzalez JC, Kenkel JA, Hartmann FJ, et al. Immune-stimulating antibody conjugates elicit robust myeloid activation and durable antitumor immunity. *Nat Cancer.* 2021;2(1):18-33.
38. Arlauckas SP, Garris CS, Kohler RH, Kitaoka M, Cuccarese MF, Yang KS, et al. In vivo imaging reveals a tumor-associated macrophage-mediated resistance pathway in anti-PD-1 therapy. *Sci Transl Med.* 2017;9(389).
39. Gordon SR, Maute RL, Dulken BW, Hutter G, George BM, McCracken MN, et al. PD-1 expression by tumour-associated macrophages inhibits phagocytosis and tumour immunity. *Nature.* 2017;545(7655):495-9.
40. Beatty GL, Chiorean EG, Fishman MP, Saboury B, Teitelbaum UR, Sun W, et al. CD40 agonists alter tumor stroma and show efficacy against pancreatic carcinoma in mice and humans. *Science.* 2011;331(6024):1612-6.
41. Mantovani A, Marchesi F, Malesci A, Laghi L, and Allavena P. Tumour-associated macrophages as treatment targets in oncology. *Nat Rev Clin Oncol.* 2017;14(7):399-416.
42. Kalos M, Levine BL, Porter DL, Katz S, Grupp SA, Bagg A, et al. T cells with chimeric antigen receptors have potent antitumor effects and can establish memory in patients with advanced leukemia. *Science translational medicine.* 2011;3(95):95ra73-95ra73.
43. Biglari A, Southgate TD, Fairbairn LJ, and Gilham DE. Human monocytes expressing a CEA-specific chimeric CD64 receptor specifically target CEA-expressing tumour cells in vitro and in vivo. *Gene Ther.* 2006;13(7):602-10.
44. Morrissey MA, Williamson AP, Steinbach AM, Roberts EW, Kern N, Headley MB, et al. Chimeric antigen receptors that trigger phagocytosis. *Elife.* 2018;7.

45. Oslowski CM, and Urano F. Measuring ER stress and the unfolded protein response using mammalian tissue culture system. *Methods Enzymol.* 2011;490:71-92.

**Figure legends**

*Fig. 1: IgM-induced signaling elicits cytotoxic response in macrophages and can be integrated to a CAR design:* **A.** illustration of experimental setting**. B**. B16F10 tumor size ($mm^2$) in mice following prophylactic immunization with MoDC pulsed with tumor cell coated with allogeneic IgG or IgM (n=4). **C**. Mean percentages of B16F10 melanoma cells stained for Annexin V/PI incubated with allogenic IgG and IgM following incubation with MoDC (n=5). **D-E**. Mean levels of Granzyme B and NO (**D**) and proinflammatory cytokines (**E**) in the supernatants of MoDC following overnight activation with IgG and IgM immune complexes. (n=5). **F**. Mean fluorescent intensity of MAPK enzymes in MoDC following activation for 20 min with IgG and IgM tumor immune complexes (n=5). **G**. Illustration representing CAR-macrophage design. **H**. Confocal microscopy images of HEK293FT cells 24 hours post transfection with CAR plasmids and membranous wasabi. **I**. Representative FACS analysis of HEK239FT cells 24 hours post transfection with CAR plasmids. Results are from one representative experiment out of at least three performed. Statistical significance was calculated using non-parametric t test (*** denote $p<0.001$, **** denote $p<0.0001$).

*Fig. 2: scFv are not expressed by myeloid cells.* **A**. Confocal microscopy images of DC 2.4 cells 24 hours post transfection with CAR plasmids and membranous wasabi. **B**. Representative FACS analysis of DC 2.4 cells 24 hours post transfection with CAR plasmids. **C**. Percentages of transfected cells 24 hours following transfection (n=4). **D**. Confocal microscopy images of THP-1 cells 72 hours post infection with CAR-C5α-mCherry and tdTomato plasmids. **E**. Percentages of transfected human cells 72 hours following transduction (n=4). **F-G**. Representative confocal microscopy (**F**) and mean percentages (**G**) of cells expressing chimeric molecules 24 hours after transfection. **H-I**. Representative confocal microscopy (**H**) and mean percentages of cells (**I**) expressing chimeric molecules 24 hours following transfection (n=4). Results are from one representative experiment out of at least three performed. Statistical significance was calculated using non-parametric t test (*** denote $p<0.001$, **** denote $p<0.0001$).

*Fig. 3: Both VH and VL domains prevent expression of ScFv in myeloid cells.* **A**. Confocal microscopy images of DC 2.4 cells 24 hours post transfection with αCD19-scFv GFP plasmid. **B**. Geometric mean of GFP positive cells 24hr post transfection with different αCD19- and TA99- ScFv GFP constructs in DC2.4. (n=3) **C**. Confocal microscopy images of

HEK 293FT and DC 2.4 cells 24 hours post transfection with αCD19-variable light chain GFP plasmid. **D**. Confocal microscopy images of HEK 293FT and DC 2.4 cells 24 hours post transfection with αCD19-variable heavy chain GFP plasmid **E**. Mean percentages of cells expressing scFv fragments 24 h post transfection (n=). **F**. left: illustration of mutated variable light chain. right: confocal microscopy images of HEK 293FT and DC 2.4 cells 24 hours post transfection with αCD19- mutated (linear) variable light chain. **G**. Representative confocal images of HEK293FT and DC2.4 cells 24 hours post transfection with 1/3 fragments of αCD19-variable light chain GFP plasmid **H**. Mean percentages of GFP positive cells 24hr post transfection with different fragments of scFv-GFP in DC2.4 and RAW264.7 (n=4). Results are from one representative experiment out of at least three performed. Statistical significance was calculated using non-parametric t test (*** denote $p<0.001$, **** denote $p<0.0001$).

*Fig. 4: ScFv fragments induce ER stress in myeloid cells.* **A**. Confocal microscopy imaging of RAW 264.7 24hr post transfection with linear mRNA vectors translating to GFP and αCD19-scFv GFP. **B**. qPCR data showing relative mRNA levels in RAW 264.7 transfected with GFP, Fc receptor-GFP and αCD19-ScFv GFP. (n=3) **C**. Upper: illustration of plasmid subunits. Lower: confocal microscopy imaging of HEK293FT and RAW 264.7 24hr post transfection with T2A ribosomal skipping plasmid including ScFv. **D**. Upper: Illustration of plasmid subunits. Lower: confocal microscopy imaging of HEK293FT and RAW 264.7 24hr post transfection with plasmid containing no T2A. **E**. Confocal microscopy images of RAW264.7 cells at 6 hours and 24 hours post transfection with αCD19-ScFv GFP plasmid. **F**. Volcano plot showing differentially expressed proteins αCD19 ScFv GFP/GFP in DC 2.4 cells. **H**. Confocal microscopy images of DC2.4 stained with an ER stain, 24 hours post transfection with GFP, membranous TA99-ScFv GFP. **I**. Confocal microscopy images of DC2.4 stained for BiP 24 hours post transfection. Mean levels of phospho-JNK 6 hours following transfection. Results are from one representative experiment out of at least three performed. Statistical significance was calculated using non-parametric t test (*** denote $p<0.001$, **** denote $p<0.0001$).

*Figure 5: FcγRI can provide a scaffold for incorporating IgM-induced signaling in myeloid cells and endows them with tumor cell-specific killing ability.* **A**. Illustration of chimeric Fcγ receptor design. **B-C.** Representative FACS plots (**B**) and mean percentages (**C**) of

RAW264.7 cells expressing chimeric Fcγ receptors 24 h after transfection (n=3). **D**. Confocal microscopy images of RAW264.7 cells 24 hours post transfection with Fcγ receptors tagged with GFP and membrane tagged tdTomato. **E.** Mean percentages of BMDC 72 h post lentivirus transduction with Fcγ receptors (n=4). **F**. Confocal microscopy staining of GrB in RAW 264.7 cells co-cultured overnight with 4T1 cells expressing human $HER2^+$. **G**. Mean counts of GrB in the synapse between transduced RAW264.7 cells and the tumor cells (n=18). **H**. IncuCyte analysis of human $HER2^+$ 4T1 cells growth following incubation with transduced RAW 264.7 cells (n=6). **I**. Super-resolution microscopy of GFP-tagged chimeric FcγR and mCherry-tagged gamma chain. **J**. Confocal microscopy staining of GrB in RAW 264.7 cells co-cultured overnight with 4T1 cells expressing human $HER2^+$. **K**. IncuCyte analysis of human $HER2^+$ 4T1 cells growth following incubation with transduced RAW 264.7 cells (n=6). Results are from one representative experiment out of at least three performed. Statistical significance was calculated using non-parametric t test (*** denote $p<0.001$, **** denote $p<0.0001$).

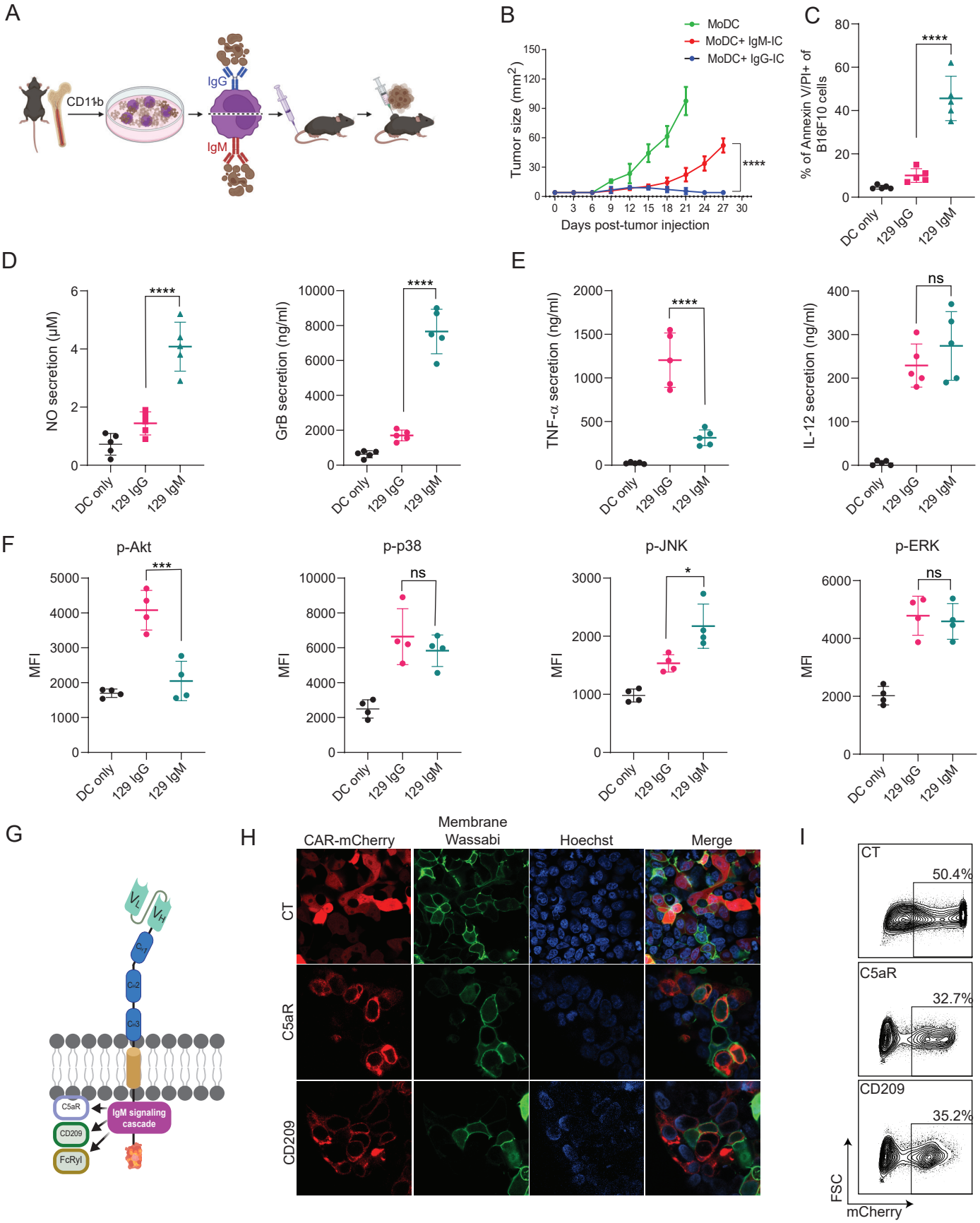
A
CD11b
IgG
IgM
B
MoDC
MoDC+ IgM-IC
MoDC+ IgG-IC
Tumor size (mm2)
Days post-tumor injection
****
C
% of Annexin V/PI+ of B16F10 cells
****
DC only
129 IgG
129 IgM
D
NO secretion (μM)
GrB secretion (ng/ml)
****
E
TNF-α secretion (ng/ml)
IL-12 secretion (ng/ml)
ns
F
p-Akt
p-p38
p-JNK
p-ERK
MFI
***
*
G
VL
VH
CH1
CH2
CH3
C5aR
CD209
FcRγI
IgM signaling cascade
H
CAR-mCherry
Membrane Wassabi
Hoechst
Merge
CT
C5aR
CD209
I
CT
50.4%
C5aR
32.7%
CD209
35.2%
FSC
mCherry

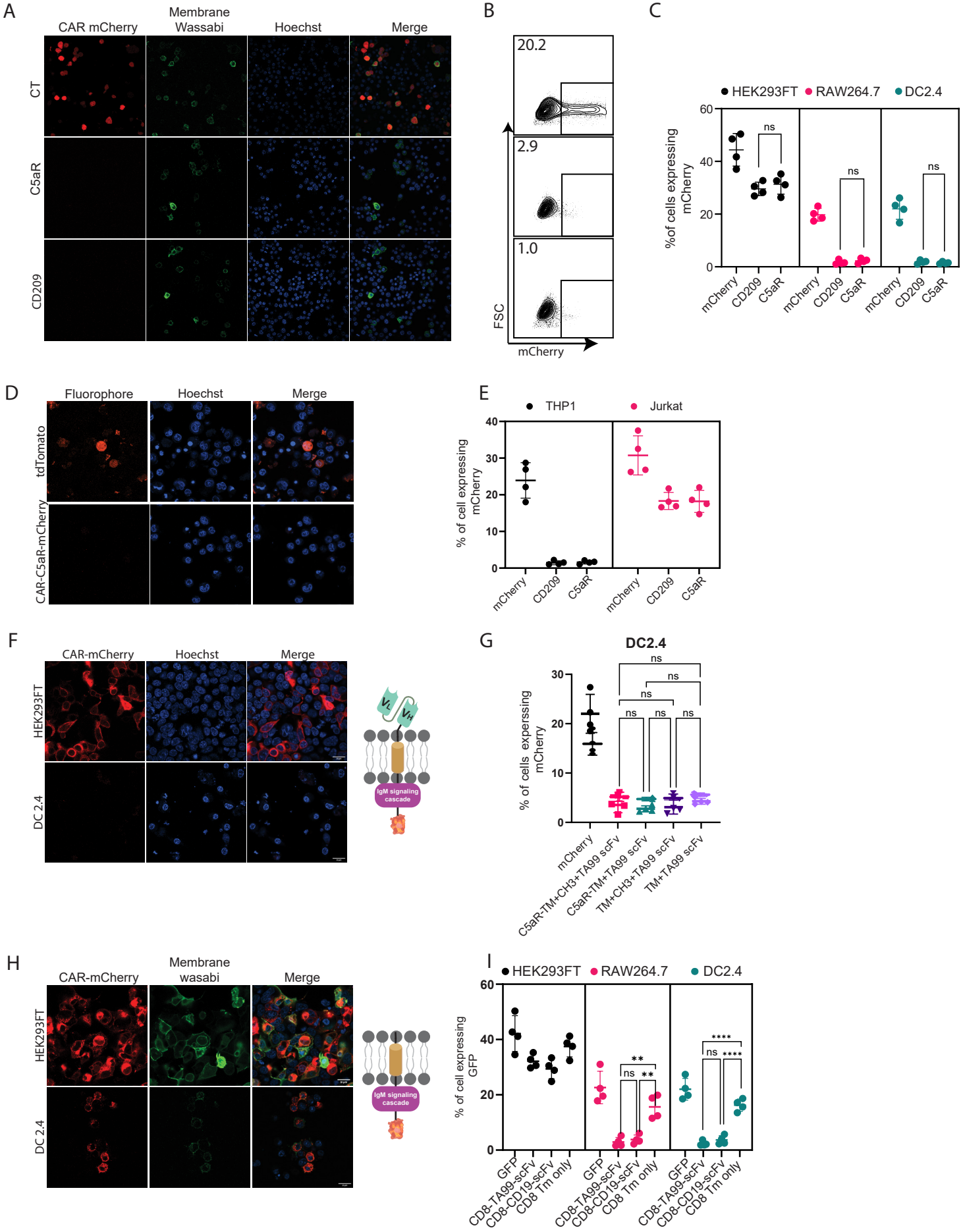
A
CAR mCherry
Membrane Wassabi
Hoechst
Merge
CT
C5aR
CD209
B
20.2
2.9
1.0
FSC
mCherry
C
HEK293FT
RAW264.7
DC2.4
%of cells expressing mCherry
ns
mCherry
CD209
C5aR
D
Fluorophore
Hoechst
Merge
tdTomato
CAR-C5aR-mCherry
E
THP1
Jurkat
% of cell expressing mCherry
F
CAR-mCherry
Hoechst
Merge
HEK293FT
DC 2.4
IgM signaling cascade
G
DC2.4
% of cells experssing mCherry
mCherry
C5aR-TM+CH3+TA99 scFv
C5aR-TM+TA99 scFv
TM+CH3+TA99 scFv
TM+TA99 scFv
H
CAR-mCherry
Membrane wasabi
Merge
HEK293FT
DC 2.4
IgM signaling cascade
I
HEK293FT
RAW264.7
DC2.4
% of cell expressing GFP
GFP
CD8-TA99-scFv
CD8-CD19-scFv
CD8 Tm only
**
****

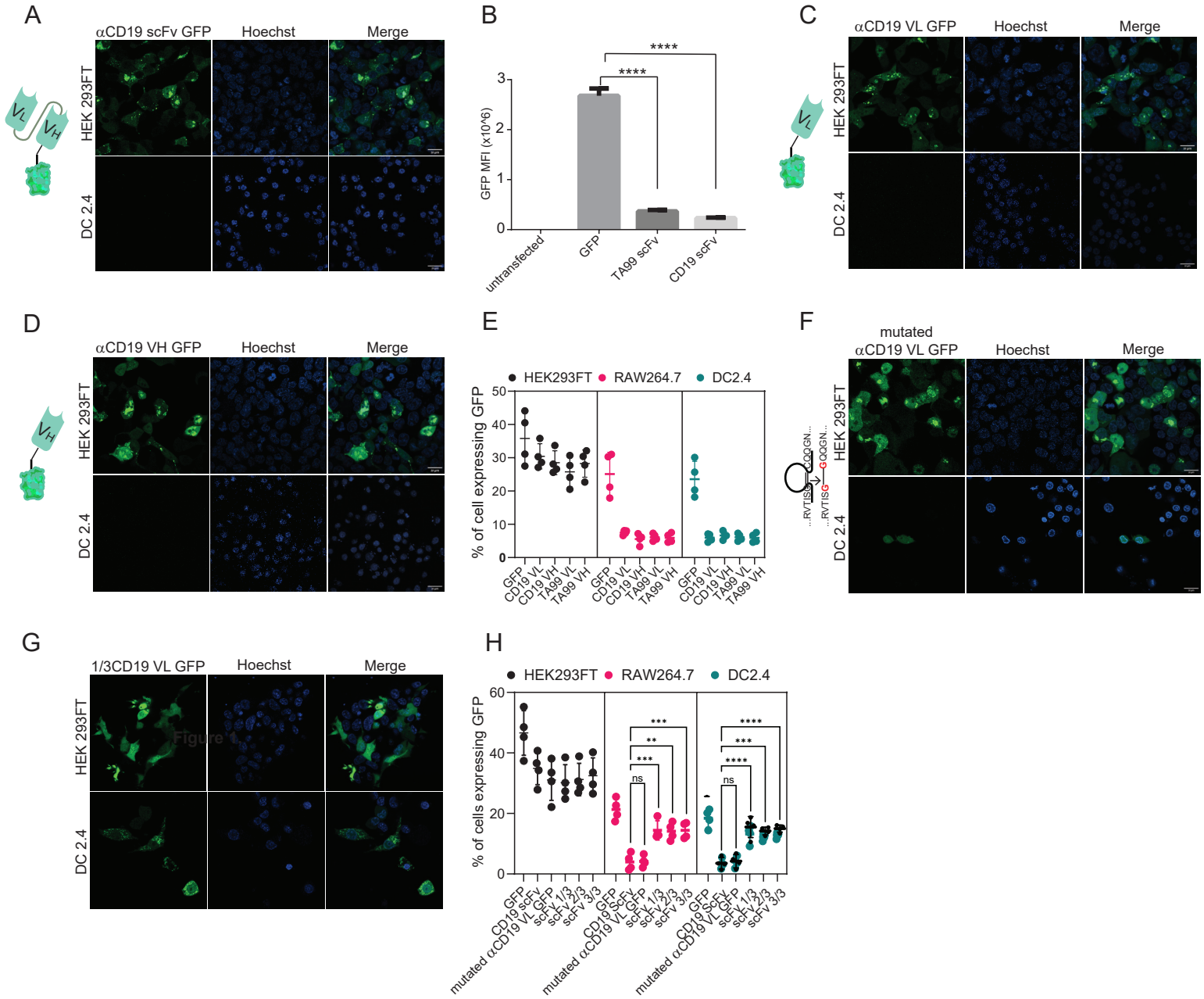
A
αCD19 scFv GFP
Hoechst
Merge
HEK 293FT
DC 2.4
B
GFP MFI (x10^6)
****
****
untransfected
GFP
TA99 scFv
CD19 scFv
C
αCD19 VL GFP
Hoechst
Merge
HEK 293FT
DC 2.4
D
αCD19 VH GFP
Hoechst
Merge
HEK 293FT
DC 2.4
E
HEK293FT
RAW264.7
DC2.4
% of cell expressing GFP
GFP
CD19 VL
CD19 VH
TA99 VL
TA99 VH
F
mutated
αCD19 VL GFP
Hoechst
Merge
HEK 293FT
DC 2.4
G
1/3CD19 VL GFP
Hoechst
Merge
HEK 293FT
DC 2.4
H
HEK293FT
RAW264.7
DC2.4
% of cells expressing GFP
***
**
***
ns
****
***
****
ns
GFP
CD19 scFv
mutated αCD19 VL GFP
scFv 1/3
scFv 2/3
scFv 3/3

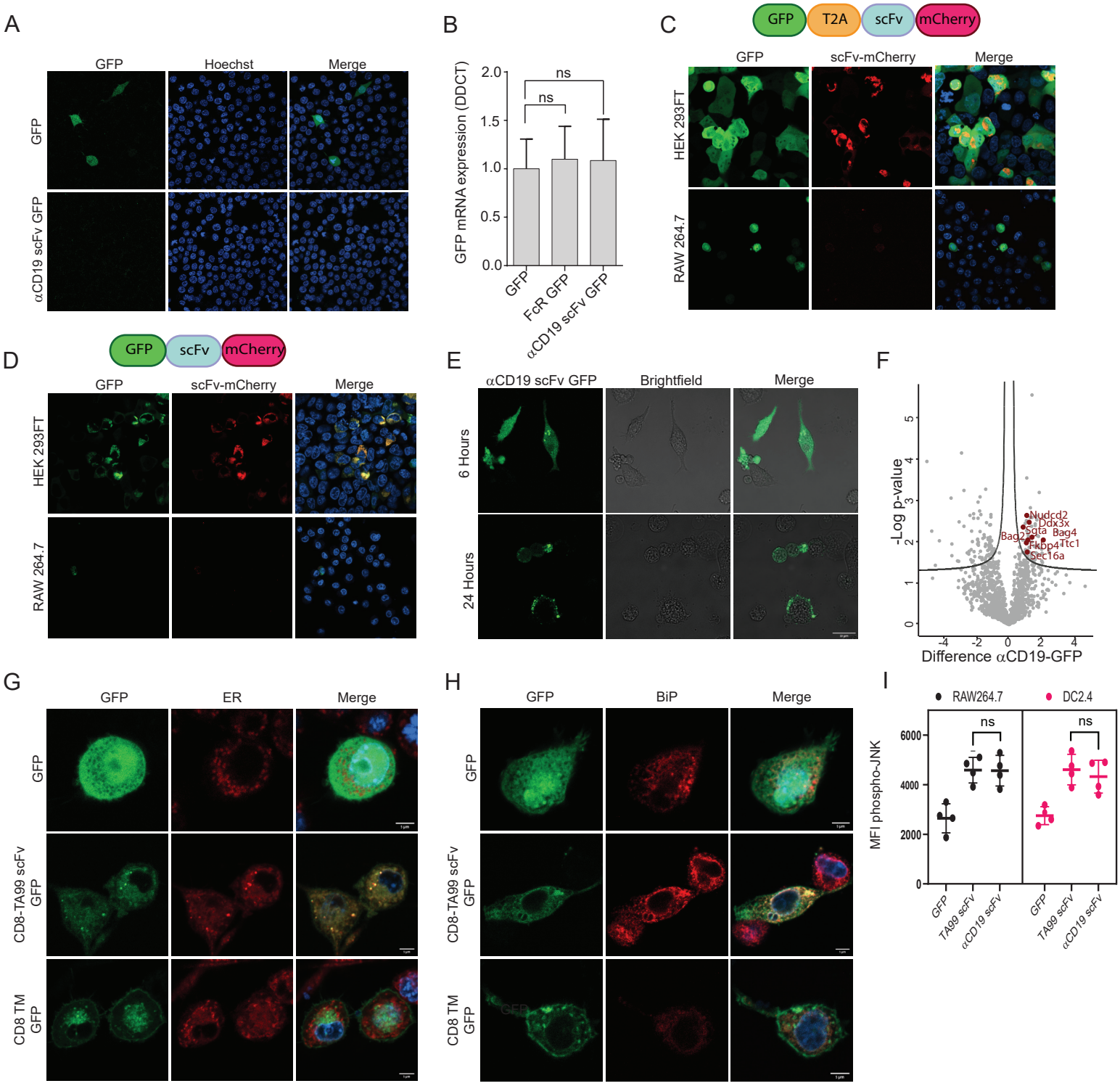
A
GFP
Hoechst
Merge
GFP
αCD19 scFv GFP
B
GFP mRNA expression (DDCT)
2.0
1.5
1.0
0.5
0.0
ns
ns
GFP
FcR GFP
αCD19 scFv GFP
C
GFP
T2A
scFv
mCherry
GFP
scFv-mCherry
Merge
HEK 293FT
RAW 264.7
D
GFP
scFv
mCherry
GFP
scFv-mCherry
Merge
HEK 293FT
RAW 264.7
E
αCD19 scFv GFP
Brightfield
Merge
6 Hours
24 Hours
F
-Log p-value
Difference αCD19-GFP
Nudcd2
Ddx3x
Sgta
Bag4
Bag2
Fkbp4
Ttc1
Sec16a
G
GFP
ER
Merge
GFP
CD8-TA99 scFv GFP
CD8 TM GFP
H
GFP
BiP
Merge
GFP
CD8-TA99 scFv GFP
CD8 TM GFP
I
RAW264.7
DC2.4
MFI phospho-JNK
6000
4000
2000
0
ns
ns
GFP
TA99 scFv
αCD19 scFv
GFP
TA99 scFv
αCD19 scFv

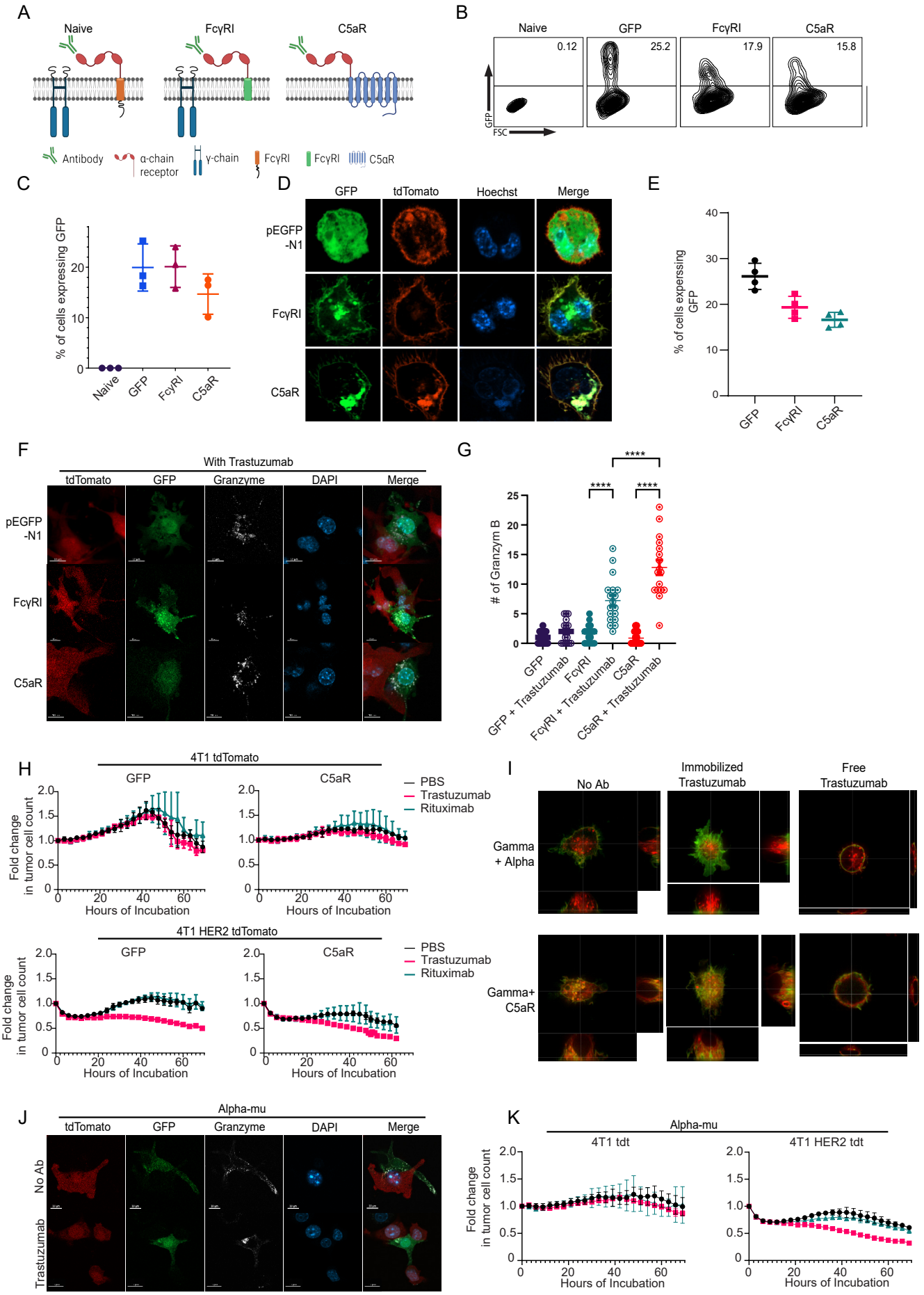
A
Naive
FcγRI
C5aR
Antibody
α-chain receptor
γ-chain
FcγRI
FcγRI
C5αR
B
Naive
GFP
FcγRI
C5aR
0.12
25.2
17.9
15.8
GFP
FSC
C
% of cells expressing GFP
Naive
GFP
FcγRI
C5aR
D
GFP
tdTomato
Hoechst
Merge
pEGFP -N1
FcγRI
C5aR
E
% of cells experssing GFP
GFP
FcγRI
C5aR
F
With Trastuzumab
tdTomato
GFP
Granzyme
DAPI
Merge
pEGFP -N1
FcγRI
C5aR
G
# of Granzym B
****
****
****
GFP
GFP + Trastuzumab
FcγRI
FcγRI + Trastuzumab
C5aR
C5aR + Trastuzumab
H
4T1 tdTomato
GFP
C5aR
PBS
Trastuzumab
Rituximab
Fold change in tumor cell count
Hours of Incubation
4T1 HER2 tdTomato
GFP
C5aR
PBS
Trastuzumab
Rituximab
Fold change in tumor cell count
Hours of Incubation
I
No Ab
Immobilized Trastuzumab
Free Trastuzumab
Gamma + Alpha
Gamma+ C5aR
J
Alpha-mu
tdTomato
GFP
Granzyme
DAPI
Merge
No Ab
Trastuzumab
K
Alpha-mu
4T1 tdt
4T1 HER2 tdt
Fold change in tumor cell count
Hours of Incubation